Studying buckling of composite rods made of hybrid carbon fiber/carbon nanotube reinforced polyimide using multiscale FEM

[a] M. Ahmadi, [a] R. Ansari, [b] H. Rouhi[*]

[a] *Department of Mechanical Engineering, University of Guilan, P.O. Box 3756, Rasht, Iran*

[b] *Department of Engineering Science, Faculty of Technology and Engineering, East of Guilan, University of Guilan, P.C. 44891-63157, Rudsar-Vajargah, Iran*

Abstract

In this paper, the buckling behavior of rods made of carbon fiber/carbon nanotube-reinforced polyimide (CF/CNT-RP) under the action of axial load is investigated based on a multiscale finite element method. A dual-step procedure is first adopted to couple the influences of micro- and nano-scale in order to obtain the equivalent elastic properties of CF/CNT-RP for various volume fractions of CF and CNT. The interphase effect between CNTs and the polymer matrix is taken into consideration. Also, dispersion of CF/CNT into the polymer matrix is assumed to be random. Then, rods with square and circular cross sections are considered whose stability characteristics are analyzed. The finite element modeling is performed using two models including a 3D brick model and a 2D beam model. Selected numerical results are given to study the effects of volume fraction of CNT/CF, interphase and geometrical properties on the axial buckling response of multiscale composite rods.

Keywords: Multiscale composite rod; Hybrid carbon nanotube/carbon fiber reinforcement; Polyimide; Buckling; Finite element method

[*] Corresponding author. Tel. /fax: +98 13 42688447

E-mail addresses:
masoud_ahmadi_pr@yahoo.com (M. Ahmadi)
r_ansari@guilan.ac.ir (R. Ansari)
h_rouhi@guilan.ac.ir (H. Rouhi)

1. Introduction

Hybrid composite materials have been the focus of several research works in recent years [1-7]. This attention is mainly attributed to the wide range of possibilities to modify the properties of such materials at different length scales. In particular, polymer matrix composites reinforced with carbon nanotubes (CNTs) and carbon fibers (CFs) have attracted a lot of attention from the research community due to their excellent mechanical and electrical properties together with multi-functionality. For example, CNT/CF/epoxy composites indicated ~30% enhancement of the interlaminar shear strength in comparison with that of CF/epoxy composites without CNTs, and demonstrated considerably improved out-of-plane electrical conductivity [1]. Alipour Skandani and Al-Haik [5] revealed that surface grown CNTs can enhance the CF-reinforced composite resistance to viscoplastic deformation. Pal and Kumar [6] showed that even at low CF content, dispersing CNTs in the CF-polymer composite significantly improves the effective electrical conductivity and electrical percolation threshold of the resulting composite. The properties and performance of CNT-reinforced composites are dependent on different parameters. Synthesizing strategy, morphology of CNTs, type of matrix (e.g. metal, polymer, etc.), dispersion of CNTs and interfacial reactions between CNTs and matrix can be mentioned as some examples. The reader is referred to [8] for more details.

Up to now, many micromechanical models have been developed to estimate the mechanical properties of CNT-reinforced composites [9-15]. Also, there are some research works in which the mechanical behaviors (e.g. vibration, buckling, bending) of structural elements made of nanocomposites have been studied [16-32].

As the lattice structure of CNTs is not incorporated into the micromechanical models, the direct application of continuum micromechanical models may lead to inaccurate results in the analysis of CNT-reinforced composites [33]. Furthermore, CNT/polymer matrix interphase region is one of the most important factors in the analysis of reinforced polymers with CNTs [34]. The interphase is formed by non-bonded van der Waals (vdW) interaction between the CNT and surrounding matrix. Therefore, multi-scale modeling approaches to consider the coupled micro- and nano-scale effects have been proposed in a number of works [35-43].

Also, there are some size-dependent generalized continuum theories to capture small-scale effects. The nonlocal, strain gradient and couple stress theories are well-known non-classical

elasticity theories capable of considering size influences at micro- and nano-scale. On the basis of nonlocal elasticity theory, the stress tensor at a reference point in a body depends not only on the strain tensor at that point, but also on the strain tensor at all other points of the body. The nonlocal parameter of this theory can be determined using experimental data or results from atomistic approaches like molecular dynamics simulations. The nonlocal theory has been applied to various problems such as buckling of microtubules and boron-nitride nanotubes embedded in elastic medium [44, 45] and bending/ buckling/ free vibration analyses of nanobeams [46, 47]. The reader is also referred to [48-52] as some examples for the applications of strain gradient and couple stress theories.

As cited, there are some papers on the finite element multiscale modeling of structural elements made of nanocomposites. However, to the authors' knowledge, the buckling behavior of rods made of CNT/CF-reinforced polyimide considering coupled effects of micro- and nano-scale based on a finite element approach has not been investigated yet. Therefore in the present paper, the multiscale buckling analysis of composite rods made of CNT/CF-reinforced polyimide is presented employing the finite element method (FEM). To achieve this aim, the elastic properties of CNT/CF-RP including Young's modulus and Poisson's ratio are first determined using a dual-step procedure. In the first step, CNTs with three values of volume fraction (1%, 3% and 5%) are randomly dispersed into the polymer matrix (polyimide). In the selected representative volume element (RVE), the interphase region between CNTs and the polymer matrix is taken into account. Then, random distribution of CFs into the CNT-reinforced polymer is modeled according to six cases of hybrid CNT/CF reinforcement. The elastic properties of composite are calculated with and without considering the interphase influence. After that, the axial buckling of rods made of CNT/CF-RP with circular and square cross sections is analyzed. The analysis is performed via two models: a 3D brick model and a 2D beam model. The effect of some important factors including interphase, volume fraction of CNT/CF and size on the critical buckling loads are investigated. Also, a comparison is made between the predictions of brick and beam models.

2. Dual-Step Multiscale Finite Element Modeling

In order to estimate the elastic constants of polyimide reinforced by carbon fibers and carbon nanotubes, a dual-step procedure is adopted herein [38]. In the first step, CNTs are dispersed into the polymer matrix (polyimide) with three volume fractions including 1%, 3% and 5%. The RVE model of this step can be observed in Fig. 1. The dispersion of CNTs is considered to be random from the viewpoints of orientation and coordinates. In addition, they are dispersed approximately homogenous without aggregation. The RVE consists of three phases: CNTs, polymer matrix and interphase. The interphase is formed due to non-bonded vdW interaction between the CNT and surrounding matrix. It is modeled as a layer developed around the CNT. Shen and Li [53, 54] showed that CNTs are transversely isotropic materials. Consequently, CNTs are modeled as transversely isotropic materials in the present finite element modeling. Also, the polymer matrix and interphase are considered as isotropic.

In the next step, CFs are distributed in the CNT-reinforced polyimide (CNT-RP) that is considered a homogenous material with the properties estimated in the first step. Six cases are studied for the hybrid reinforcement:

(0.95% CNT + 5% CF + Polyimide)
(2.85% CNT + 5% CF + Polyimide)
(4.75% CNT + 5% CF + Polyimide)
(0.9% CNT + 10% CF + Polyimide)
(2.7% CNT + 10% CF + Polyimide)
(4.5% CNT + 10% CF + Polyimide)

The RVE model of nanocomposite with random dispersion of CFs is indicated in Fig. 2. Similar to CNTs, CFs are assumed to be transversely isotropic. The Python programming language is utilized to create randomly distributed/oriented CNTs/CFs inside the RVE. It should be noted that the positions of CNTs/CFs are determined in such a way that no overlapping occurs between them.

Fig. 3 shows examples of meshed RVEs. Also, Fig. 4 represents loading and boundary conditions of RVE to obtain Young's modulus. It is assumed that the effective properties of the nanocomposite are similar to those of RVE. By measuring the fixed boundary reaction force and

calculating stress value (σ), the equivalent elastic modulus (E) of nanocomposite RVE is obtained based on Hooke's law as follows

$$E = \frac{\sigma}{\varepsilon} \tag{1}$$

where ε is the RVE strain in the load direction. Poisson's ratio is also defined as the ratio of transverse strain to axial strain. It should be noted that for each reinforcement type, the results are obtained using average values of three analyses with various random microstructures in order to reduce the effect of chance on the results because of random dispersion. Besides, the present calculations revealed that there is a negligible difference between the results from 2D and 3D RVEs. Hence, 2D RVEs are used instead of 3D ones due to the high computational cost of 3D models.

After calculating Young's modulus and Poisson's ratio of CNT/CF-RP for various reinforcement types with and without the interphase influence, the buckling analysis of rods with circular and square cross sections is performed. The finite element modeling is performed using two models: a 3D brick model and a 2D beam model as shown in Fig. 5. At the micro-scale, an 8-node biquadratic plane stress quadrilateral element is used. Also, at the macro-scale, a 3-node quadratic beam in space is used for the 2D beam model, and a 20-node quadratic brick is used for the 3D brick model.

3. Results and Discussion

First, in order to validate the proposed multiscale FEM, the present results for Young's modulus of polypropylene reinforced with randomly oriented CNTs are compared with the experimental results given in [55]. Table 1 shows the normalized Young's modulus of CNT-reinforced polypropylene for different volume fractions of CNT. It is seen that the present results are in good agreement with those reported in [55].

The material properties of composite constituents are given in Table 2. In this table, longitudinal Young's modulus (E_L), transverse Young's modulus (E_T), longitudinal Poisson's ratio (ν_L), transverse Poisson's ratio (ν_T), longitudinal shear modulus (G_L) and mass density (ρ) of CNTs, interphase, CFs and the polymer matrix are presented. The aspect ratio and diameter of

CFs are selected as 10 and 10 μm, respectively. Moreover, the aspect ratio and diameter of CNTs are taken as 100 and 0.78 nm, respectively. Also, the thickness of interphase is considered to be 0.3333 nm.

To study the mesh convergence, as an example, Young's modulus of 2.85% CNT - 5% CF - RP (without interphase) is computed with various mesh sizes as shown in Table 3. This table reveals a converged trend with mesh size becoming smaller. It is worth mentioning that the fining mesh is performed to reach a change smaller than 0.005% in the solution.

The values of equivalent Young's modulus, Poisson's ratio and mass density of CNT/CF-reinforced polyimide for different volume fractions of CNT/CF are tabulated in Table 4. The results of this table are generated with and without considering interphase in order to show such an effect. The elastic properties of pristine material (polyimide) are also given so as to study the effect of reinforcement. According to the results, Young's modulus computed with taking the interphase effect into account is larger than that obtained without considering the interphase effect. For example, there is 4.5% increase in the value of Young's modulus of (4.75% CNT + 5% CF + Polyimide) when the interphase is considered.

As expected, reinforcing polyimide with CNT/CF results in increasing the elastic modulus. For instance, when 5% CNT is added to the polymer matrix, an 88% increase in the elastic modulus of resulting composite material is observed. Also, the increase reaches 133% in the case of (4.5% CNT + 10% CF + Polyimide). It is also observed that the effect of reinforcement on Poisson's ratio is insignificant.

Now, the buckling results of composite rods made of CNT/CF-RP are given and discussed. It is considered that the rods are under an axial point load applied to the center of cross section (circular and square). Furthermore, the boundary condition of rods is assumed to be clamped-free.

In Table 5, the results of multiscale FEM are compared to those obtained from Euler's formula. The critical load based on Euler's formula is given by

$$F_{cr} = \frac{\pi^2 EI}{(KL)^2} \tag{2}$$

where E, I, L and K denote elastic modulus, second moment of inertia of the cross section, length and effective length factor of the rod, respectively. The comparison is done for rods with

both circular and square cross sections using 3D brick and 2D beam models. Also, various values of diameter are considered. It is observed that the finite element results agree well with the ones obtained based on Euler's formula.

Tables 6 and 7 show the critical buckling loads of rods made of different materials with circular and square cross sections, respectively. The results of these tables are obtained by both brick and beam models. The effects of interphase, material and geometrical properties on the buckling behavior of rods can be investigated herein. It is seen that by the hybrid CNT/CF reinforcement, the resistance of rods to applied axial load improves significantly. For example, for the cylindrical rod with the radius equal to 20 mm, the critical buckling load 123% increases when the material is changed from polyimide to (4.5% CNT + 10% CF + Polyimide).

Besides, the interphase effect on the calculated critical buckling loads is observed from Tables 6 and 7. For example, for the square rod made of (4.75% CNT + 5% CF + Polyimide) with the diameter equal to 40 mm, the critical buckling load calculated with considering the interphase is 4% larger than that obtained without taking the interphase into consideration.

Also, comparison between the results generated based on the 3D brick model and 2D beam model indicates that the discrepancy between the predictions of two models can be neglected for small values of radius/diameter. However, the difference increases as the radius/diameter gets larger.

4. Conclusion

A dual-step multiscale FE procedure was employed in this work in order to investigate the buckling behavior of rods made of polyimide reinforced with the combination of CNT and CF. To this end, the elastic modulus and Poisson’s ratio of CNT/CF-RP for various reinforcement types were first calculated. It was shown that the elastic modulus considerably increases when polyimide is reinforced by the combination of CNT and CF. Moreover, the effect of interphase on the results was examined. It was indicated that the elastic modulus obtained with considering the interphase effect is larger than that obtained without the interphase effect. It was also concluded that the effect of reinforcement on Poisson’s ratio is insignificant. After determining the elastic properties of CNT/CF-RP, the critical buckling loads of hybrid polymer composite rods with circular and square cross sections were calculated. The results revealed that the

buckling behavior of rods is significantly affected by the type of reinforcement. It was observed that there is a notable improvement in the resistance of rods to the buckling when their material is a hybrid CNT/CF-polyimide composite instead of neat polyimide. A comparison was also made between the results of 3D brick and 2D beam models.

References

[1] Bekyarova, E., Thostenson, E. T., Yu, A., Kim, H., Gao, J., Tang, J., Hahn, H. T., Chou, T. W., Itkis, M. E., and Haddon, R. C., "Multiscale Carbon Nanotube−Carbon Fiber Reinforcement for Advanced Epoxy Composites," *Langmuir*, **23**, pp. 3970–3974 (2007).

[2] Kepple, K. L., Sanborn, G. P., Lacasse, P. A., Gruenberg, K. M., and Ready, W. J., "Improved fracture toughness of carbon fiber composite functionalized with multi walled carbon nanotubes," *Carbon*, **46**, pp. 2026–2033 (2008).

[3] Sawi, I. E., Olivier, P. A., Demont, P., and Bougherara, H.., "Processing and electrical character-ization of a unidirectional CFRP compositefilled with double walled carbon nano-tubes," *Compos. Sci. Technol.*, **73**, pp. 19–26 (2012).

[4] Tehrani, M., Safdari, M., Boroujeni, A. Y., Razavi, Z., Case, S. W., Dahmen, K., Garmestani, H., and Al-Haik, M. S., "Hybrid carbon fiber/carbon nanotube composites for structural damping applications," *Nanotechnology*, **24**, 155704 (2013).

[5] Alipour Skandani, A., and Al-Haik, M., "Viscoplastic characterization and modeling of hybrid carbon fiber/carbon nanotubes reinforced composites," *Compos. Part B*, **99**, pp. 63–74 (2016).

[6] Pal, G., and Kumar, S., "Multiscale modeling of effective electrical conductivity of short carbon fiber-carbon nanotube-polymer matrix hybrid composites," *Mater. Des.*, **89**, pp. 129–136 (2016).

[7] Zhou, H. W., Mishnaevsky Jr., L., Yi, H. Y., Liu, Y. Q., Hua, X., Warrier, A., and Dai, G. M., "Carbon fiber/carbon nanotube reinforced hierarchical composites: Effect of CNT distribution on shearing strength," *Compos. Part B*, **88**, pp. 201–211 (2016).

[8] Mittal, G., Dhand, V., Rhee, K. Y., Park, S.-J., and Lee, W. R., "A review on carbon nanotubes and graphene as fillers in reinforced polymer nanocomposites," *J. Indust. Eng. Chem.*, **21**, pp. 11-25 (2015).

[9] Seidel, G. D., and Lagoudas, D. C., "Micromechanical analysis of the effective elastic properties of carbon nanotube reinforced composites," *Mech. Mater.*, **38**, pp. 884–907 (2006).

[10] Giannopoulos, G. I., Georgantzinos, S. K., and Anifantis, N. K., "A Semi-Continuum Finite Element Approach to Evaluate the Young's Modulus of Single-Walled Carbon Nanotube Reinforced Composites," *Compos. Part B*, **41**, pp. 594-601 (2010).

[11] Loos, M. R., and Manas-Zloczower, I., "Micromechanical models for carbon nanotube and cellulose nanowhisker reinforced composites," *Polymer Eng. Sci.*, **53**, pp. 882–887 (2013).

[12] Ansari, R., and Hassanzadeh Aghdam, M. K., "Micromechanics-based viscoelastic analysis of carbon nanotube-reinforced composites subjected to uniaxial and biaxial loading," *Compos. Part B*, **90**, pp. 512-522 (2016).

[13] Ansari, R., and Hassanzadeh Aghdam, M. K., "Micromechanical characterizing elastic, thermoelastic and viscoelastic properties of functionally graded carbon nanotube reinforced polymer nanocomposites," *Meccanica*, **52**, pp. 1625-1640 (2017).

[14] Alva, A., Bhagat, A., and Raja, S., "Effective Moduli Evaluation of Carbon Nanotube Reinforced Polymers Using Micromechanics," *Mech. Adv. Mater. Struct.*, **22**, pp. 819-828 (2015).

[15] Ansari, R., Hassanzadeh Aghdam, M. K., and Mahmoodi, M. J., "Three-dimensional micromechanical analysis of the CNT waviness influence on the mechanical properties of polymer nanocomposites," *Acta Mech.*, **227**, pp. 3475–3495 (2016).

[16] Wattanasakulpong, N., and Ungbhakorn, V., "Analytical Solutions for Bending, Buckling and Vibration Responses of Carbon Nanotube-Reinforced Composite Beams Resting on Elastic Foundation," *Comput. Mater. Sci.*, **71**, pp. 201-208 (2013).

[17] Lin, F., and Xiang, Y., "Vibration Analysis of Carbon Nanotube Reinforced Composite Plates," *Appl. Mech. Mater.*, **553**, pp. 681-686 (2014).

[18] Abdollahzadeh Shahrbabaki, E., and Alibeigloo, A., "Three-Dimensional Free Vibration of Carbon Nanotube-Reinforced Composite Plates with Various Boundary Conditions Using Ritz Method," *Compos. Struct.*, **111**, pp. 362-370 (2014).

[19] Ansari, R., Faghih Shojaei, M., Mohammadi, V., and Sadeghi, F., "Nonlinear forced vibration analysis of functionally graded carbon nanotube-reinforced composite Timoshenko beams," *Compos. Struct.*, **113**, pp. 316–327 (2014).

[20] Ansari, R., Hasrati, E., Faghih Shojaei, M., Gholami, R., and Shahabodini, A., "Forced vibration analysis of functionally graded carbon nanotube-reinforced composite plates using a numerical strategy," *Physica E*, **69**, pp. 294–305 (2015).

[21] Wu, H. L., Yang, J., and Kitipornchai, S., "Imperfection sensitivity of postbuckling behaviour of functionally graded carbon nanotube-reinforced composite beams," *Thin-Walled Struct.*, **108**, pp. 225–233 (2016).

[22] Ansari, R., Shahabodini, A., and Faghih Shojaei, M., "Vibrational analysis of carbon nanotube-reinforced composite quadrilateral plates subjected to thermal environments using a weak formulation of elasticity," *Compos. Struct.*, **139**, pp. 167–187 (2016).

[23] Mirzaei, M., and Kiani, Y., "Free vibration of functionally graded carbon-nanotube-reinforced composite plates with cutout," *Beilstein J. Nanotechnol.*, **7**, pp. 511–523 (2016).

[24] Ansari, R., Pourashraf, T., Gholami, R., and Shahabodini, A., "Analytical solution for nonlinear postbuckling of functionally graded carbon nanotube-reinforced composite shells with piezoelectric layers," *Compos. Part B*, **90**, pp. 267–277 (2016).

[25] Ghorbani Shenas, A., Malekzadeh, P., and Ziaee, S., "Vibration analysis of pre-twisted functionally graded carbon nanotube reinforced composite beams in thermal environment," *Compos. Struct.*, **162**, pp. 325–340 (2017).

[26] Gholami, R., Ansari, R., and Gholami, Y., "Nonlinear resonant dynamics of geometrically imperfect higher-order shear deformable functionally graded carbon-nanotube reinforced composite beams," *Compos. Struct.*, **174**, pp. 45-58 (2017).

[27] Gholami, R., and Ansari, R., "The effect of initial geometric imperfection on the nonlinear resonance of functionally graded carbon nanotube-reinforced composite rectangular plates," *Appl. Math. Mech.*, **39**, pp. 1219–1238 (2018).

[28] Gholami, R., and Ansari, R., "Nonlinear harmonically excited vibration of third-order shear deformable functionally graded graphene platelet-reinforced composite rectangular plates," *Eng. Struct.*, **156**, pp. 197-209 (2018).

[29] Gholami, R., and Ansari, R., "Large deflection geometrically nonlinear analysis of functionally graded multilayer graphene platelet-reinforced polymer composite rectangular plates," *Compos. Struct.*, **180**, pp. 760-771 (2018).

[30] Gholami, R., Ansari, R., and Gholami, Y., "Numerical study on the nonlinear resonant dynamics of carbon nanotube/fiber/polymer multiscale laminated composite rectangular plates with various boundary conditions," *Aerosp. Sci. Technol.*, **78**, pp. 118-129 (2018).

[31] Gholami, R., and Ansari, R., "Nonlinear bending of third-order shear deformable carbon nanotube/fiber/polymer multiscale laminated composite rectangular plates with different edge supports," *Eur. Phys. J. Plus*, **133**, p. 282 (2018).

[32] Gholami, R., and Ansari, R., "Geometrically nonlinear resonance of higher-order shear deformable functionally graded carbon-nanotube-reinforced composite annular sector plates excited by harmonic transverse loading," *Eur. Phys. J. Plus*, **133**, p. 56 (2018).

[33] Odegard, G. M., Gates, T. S., Wise, K. E., Park, C., and Siochi, E. J., "Constitutive modeling of nanotube-reinforced polymer composites," *Compos. Sci. Technol.*, **63**, pp. 1671–87 (2003).

[34] Tsai, J. L., Tzeng, S. H., and Chiu, Y. T., "Characterizing elastic properties of carbon nanotubes/polyimide nanocomposites using multi-scale simulation," *Compos. Part B,* **41**, pp. 106–115 (2010).

[35] Shokrieh, M. M., and Rafiee, R., "Stochastic multi-scale modeling of CNT/polymer composites," *Comput. Mater. Sci.,* **50**, pp. 437–446 (2010).

[36] Joshi, U. A., Sharma, S. C., and Harsha, S. P., "A multiscale approach for estimating the chirality effects in carbon nanotube reinforced composites," *Physica E,* **45**, pp. 28–35 (2012).

[37] Vu-Bac, N., Rafiee, R., Zhuang, X., Lahmer, T., and Rabczuk, T., "Uncertainty quantification for multiscale modeling of polymer nanocomposites with correlated parameters," *Compos. Part B,* **68**, pp. 446–464 (2015).

[38] Ahmadi, M., Ansari, R., and Rouhi, H., "Multi-scale bending, buckling and vibration analyses of carbon fiber/carbon nanotube-reinforced polymer nanocomposite plates with various shapes," *Physica E,* **93**, pp. 17–25 (2017).

[39] Ahmadi, M., Ansari, R., and Hassanzadeh-Aghdam, M. K., "Low velocity impact analysis of beams made of short carbon fiber/carbon nanotube-polymer composite: A hierarchical finite element approach," *Mech. Adv. Mater. Struct.,* https://doi.org/10.1080/15376494.2018.1430276 (2018).

[40] Ahmadi, M., Ansari, R., and Rouhi, H., "Free and forced vibration analysis of rectangular/circular/annular plates made of carbon fiber-carbon nanotube-polymer hybrid composites," *Sci. Eng. Compos. Mater.,* https://doi.org/10.1515/secm-2017-0279 (2018).

[41] Ahmadi, M., Ansari, R., and Rouhi, H., "On the free vibrations of piezoelectric carbon nanotube-reinforced microbeams: a multiscale finite element approach," *Iranian J. Sci. Technol. Trans. Mech. Eng.,* https://doi.org/10.1007/s40997-018-0157-x (2018).

[42] Ahmadi, M., Ansari, R., and Rouhi, S., "Fracture behavior of the carbon nanotube/carbon fiber/polymer multiscale composites under bending test – A stochastic finite element method," *Mech. Adv. Mater. Struct.,* https://doi.org/10.1080/15376494.2018.1432790 (2018).

[43] Ahmadi, M., Ansari, R., and Rouhi, H., "Free vibration analysis of carbon fiber-carbon nanotube-polymer matrix composite plates by a finite element-based multi-scale modeling approach," *J. Multiscale Model.*, **9**, 1850002 (2018).

[44] Civalek, Ö., and Demir, Ç., "A simple mathematical model of microtubules surrounded by an elastic matrix by nonlocal finite element method," *Appl. Math. Comput.*, **289**, pp. 335-352 (2016).

[45] Mercan, K., and Civalek, Ö., "DSC method for buckling analysis of boron nitride nanotube (BNNT) surrounded by an elastic matrix," *Compos. Struct.*, **143**, pp. 300–309 (2016).

[46] Refaeinejad, V., Rahmani, O., and Hosseini, S. A. H., "An analytical solution for bending, buckling, and free vibration of FG nanobeam lying on Winkler-Pasternak elastic foundation using different nonlocal higher order shear deformation beam theories," *Scientia Iranica F*, **24**, pp. 1635-1653 (2017).

[47] Norouzzadeh, A., Ansari, R., and Rouhi, H., "Isogeometric vibration analysis of small-scale Timoshenko beams based on the most comprehensive size-dependent theory," *Scientia Iranica F*, **25**, pp. 1864-1878 (2018).

[48] Akgöz, B., and Civalek, Ö., "Buckling analysis of cantilever carbon nanotubes using the strain gradient elasticity and modified couple stress theories," *J. Comput. Theor. Nanosci.*, **8**, pp. 1821-1827 (2011).

[49] Chen, W. J., and Li, X. P., "Size-dependent free vibration analysis of composite laminated Timoshenko beam based on new modified couple stress theory," *Arch. Appl. Mech.*, **83**, pp. 431–444 (2013).

[50] Akgoz, B., and Civalek, Ö., "Bending analysis of embedded carbon nanotubes resting on an elastic foundation using strain gradient theory," *Acta Astronautica*, **119**, pp. 1–12 (2016).

[51] Karimzadeh, A., and Ahmadian, M. T., "Vibrational characteristics of size dependent vibrating ring gyroscope," *Scientia Iranica B*, DOI: 10.24200/SCI.2018.20495 (2018).

[52] Jafari-Talookolaei, R. -A., Ebrahimzade, N., Rashidi-Juybari, S., and Teimoori, K., "Bending and vibration analysis of delaminated Bernoulli-Euler microbeams using the modified couple stress," *Scientia Iranica B,* **25**, pp. 675-688 (2018).

[53] Shen, L., and Li, J., "Transversely isotropic elastic properties of single-walled carbon nanotubes," *Phys. Rev. B*, **69**, 045414 (2004).

[54] Shen, L., and Li, J., "Transversely isotropic elastic properties of multiwalled carbon nanotubes," *Phys. Rev. B*, **71**, 035412 (2005).

[55] Selmi, A., Friebel, C., Doghri, I., and Hassis, H., "Prediction of the elastic properties of single walled carbon nanotube reinforced polymers: A comparative study of several micromechanical models," *Compos. Sci. Technol.,* **67**, pp. 2071–2084 (2007).

[56] Kulkarni, M., Carnahan, D., Kulkarni,K., Qian, D., and Abot, J. L., "Elastic response of a carbon nanotube fiber reinforced polymeric composite: A numerical and experimental study," *Compos. Part B,* **41**, pp. 414–421 (2010).

[57] Odegard, G. M., Clancy, T. C., and Gates, T. S., "Modeling of the mechanical properties of nanoparticle/polymer composites," *Polymer*, **46**, pp. 553–562 (2005).

Biographies:

Masoud Ahmadi received his BSc and MSc degrees in Mechanical Engineering, in 2013 and 2016, respectively, from the Razi University and University of Guilan, Iran. His research interests include finite element analysis, structural analysis and biomechanics.

Reza Ansari received his PhD degree, in 2008, from the University of Guilan, Iran, where he is currently faculty member in the Department of Mechanical Engineering. He was also a visiting fellow at Wollongong University, Australia, from 2006-2007. He has authored numerous refereed journal papers and book chapters. His research interests include computational nano- and micro-mechanics, advanced numerical techniques, nonlinear analyses and prediction of the mechanical behavior of smart composite/FGM shell-type structures.

Hessam Rouhi received his PhD degrees in Mechanical Engineering, in 2016, from the University of Guilan, Iran. He is currently faculty member in the Department of Engineering Science, Faculty of Technology and Engineering, East of Guilan, University of Guilan. His research interests include computational micro- and nano-mechanics and the mechanical behavior of structures, including buckling and vibration.

Table captions:

Table 1: Dimensionless Young's modulus of CNT-reinforced polypropylene

Table 2: Material properties of CNT, interphase, CF and polyimide

Table 3: Mesh convergence study in the case of 2.85% CNT - 5% CF-RP

Table 4: Equivalent Young's modulus, Poisson's ratio and mass density of polyimide reinforced with CNT/CF

Table 5: Comparison between the results of present multiscale FEM and those of Euler's formula for th buckling of rods with circular and square cross sections

Table 6: Critical buckling load (N) of rods with circular cross section

Table 7: Critical buckling load (N) of rods with square cross section

Figure captions:

Figure 1: RVE model of composite with random CNT distribution

Figure 2: RVE model of composite with random CF distribution

Figure 3: Examples of meshed RVEs for a) CNT-reinforced polyimide b) CF-reinforced polyimide

Figure 4: Stress distribution contour (tensile test for obtaining elastic modulus of nanocomposite)

Figure 5: a) 3D brick and b) 2D beam models for the buckling analysis of rods

Table 1: Dimensionless Young's modulus of CNT-reinforced polypropylene

CNT volume fraction (%)	Present FEM	Experiment [55]	Difference percentage
1.6	1.161	1.19	2.4
3.2	1.319	1.29	2.2
4.8	1.526	1.39	9.8

Table 2: Material properties of CNT, interphase, CF and polyimide

Material	E_L (GPa)	E_T (GPa)	ν_L	ν_T	G_L (GPa)	ρ (Kg/m^3)
CNT [34]	1382.5	645	0.272	0.2	1120	1300
Interphase [34]	19.29	19.29	0.34	0.34	7.2	1305
CF [56]	294	18.5	0.27	0.3	25	1760
Polyimide [57]	4.2	4.2	0.4	0.4	1.5	1310

Table 3: Mesh convergence study in the case of 2.85% CNT - 5% CF-RP

No. of Elements	E (GPa)	**Error (%)**
3933	7.0723	0.54
6963	7.0568	0.32
13808	7.0456	0.16
22834	7.0407	0.09
29953	7.0378	0.05
43499	7.0365	0.03
52276	7.0357	0.02
68465	7.0346	0.00
83270	7.0343	0.00
129724	7.0343	0.00

Table 4: Equivalent Young's modulus, Poisson's ratio and mass density of polyimide reinforced with CNT/CF

Material	E (GPa)	ν	ρ (Kg/m^3)
Polyimide	4.200	0.400	1310.00
1% CNT-RP (without interphase)	4.786	0.399	1309.90
1% CNT-RP (with interphase)	4.830	0.399	1309.86
3% CNT-RP (without interphase)	6.223	0.398	1309.70
3% CNT-RP (with interphase)	6.411	0.397	1309.57
5% CNT-RP (without interphase)	7.554	0.396	1309.50
5% CNT-RP (with interphase)	7.898	0.395	1309.29
0.95 % CNT- 5% CF-RP (without interphase)	5.434	0.397	1332.41
0.95% CNT- 5% CF-RP (with interphase)	5.483	0.397	1332.36
2.85% CNT - 5% CF-RP (without interphase)	7.034	0.396	1332.22
2.85% CNT- 5% CF-RP (with interphase)	7.242	0.395	1332.09
4.75% CNT - 5% CF-RP (without interphase)	8.505	0.394	1332.03
4.75% CNT- 5% CF-RP (with interphase)	8.884	0.393	1331.82
0.9% CNT - 10% CF-RP (without interphase)	6.036	0.395	1354.91
0.9% CNT- 10% CF-RP (with interphase)	6.090	0.395	1354.87
2.7 % CNT- 10% CF-RP (without interphase)	7.787	0.394	1354.73
2.7% CNT- 10% CF-RP (with interphase)	8.015	0.393	1354.61
4.5% CNT- 10% CF-RP (without interphase)	9.388	0.392	1354.55
4.5% CNT- 10% CF-RP (with interphase)	9.798	0.391	1354.36

Table 5: Comparison between the results of present multiscale FEM and those of Euler's formula for the buckling of rods with circular and square cross sections

rods with circular cross section				**rods with square cross section**			
d	3D Brick	2D Beam	Euler's critical load	d	3D Brick	2D Beam	Euler's critical load
2 mm	13.057	13.013	13.023	2 mm	1.3842	1.3814	1.3817
5 mm	509.53	506.24	508.70	4 mm	22.176	22.084	22.108
10 mm	7804.8	7984.2	8139.148	10 mm	862.14	857.78	863.59

Table 6: Critical buckling load (N) of rods with circular cross section

Material	r (mm)	3D Brick		2D Beam	
		Without interphase	With interphase	Without interphase	With interphase
Polyimide	1	0.81499		0.81376	
	2	13.057		13.013	
	5	509.53		506.24	
	10	7804.8		7984.2	
	20	102384		120846	
1% CNT-RP	1	0.92870	0.93723	0.92730	0.93582
	2	14.879	15.015	14.828	14.964
	5	580.62	585.96	576.87	582.18
	10	8893.7	8975.5	9098.2	9181.8
	20	116669	117742	137706	138972
3% CNT-RP	1	1.2075	1.2440	1.2057	1.2421
	2	19.346	19.930	19.280	19.863
	5	754.95	777.76	750.08	772.74
	10	11564	11913	11830	12187
	20	151699	156282	179053	184462
5% CNT-RP	1	1.4658	1.5326	1.4636	1.5303
	2	23.484	24.553	23.404	24.470
	5	916.43	958.16	910.51	951.97
	10	14037	14677	14360	15014
	20	184145	192531	217349	227247
0.95% CNT- 5% CF-RP	1	1.0544	1.0639	1.0528	1.0623
	2	16.893	17.045	16.836	16.988
	5	659.23	665.18	654.98	660.89
	10	10098	10189	10330	10423
	20	132466	133660	156351	157761
2.85% CNT- 5% CF-RP	1	1.3649	1.4053	1.3628	1.4031
	2	21.867	22.514	21.793	22.437
	5	853.34	878.57	847.83	872.90
	10	13071	13458	13372	13767
	20	171469	176540	202388	208372
4.75% CNT- 5% CF-RP	1	1.6503	1.7239	1.6479	1.7213
	2	26.440	27.618	26.350	27.525
	5	1031.8	1077.8	1025.1	1070.8
	10	15805	16509	16168	16888
	20	207328	216567	244712	255617
0.9% CNT- 10% CF-RP	1	1.1713	1.1817	1.1695	1.1799
	2	18.765	18.932	18.701	18.868
	5	732.27	738.82	727.54	734.05

	10	11217	11317	11474	11577
	20	147141	148457	173672	175226
2.7% CNT- 10%CF-RP	1	1.5110	1.5553	1.5087	1.5529
	2	24.208	24.917	24.126	24.832
	5	944.69	972.35	938.59	966.08
	10	14470	14894	14803	15237
	20	189825	195383	224053	230614
4.5% CNT- 10% CF-RP	1	1.8217	1.9012	1.8189	1.8984
	2	29.185	30.460	29.086	30.356
	5	1138.9	1188.7	1131.6	1181.0
	10	17445	18207	17847	18626
	20	228853	238848	270119	281915

Table 7: Critical buckling load (N) of rods with square cross section

Material	**d** (mm)	**3D Brick**		**2D Beam**	
		Without interphase	**With interphase**	**Without interphase**	**With interphase**
Polyimide	2	1.3842		1.3814	
	4	22.176		22.084	
	10	862.14		857.78	
	20	12851		13453	
	40	183615		199463	
1% CNT-RP	2	1.5773	1.5918	1.5741	1.5886
	4	25.270	25.502	25.165	25.397
	10	982.43	991.46	977.46	986.45
	20	14644	14778	15330	15471
	40	209234	211157	227293	229382
3% CNT-RP	2	2.0509	2.1129	2.0467	2.1086
	4	32.857	33.850	32.721	33.710
	10	1277.4	1316.0	1270.9	1309.3
	20	19041	19616	19933	20535
	40	272056	280275	295538	304466
5% CNT-RP	2	2.4896	2.6029	2.4845	2.5976
	4	39.885	41.701	39.720	41.528
	10	1550.6	1621.2	1542.8	1613.0
	20	23113	24166	24196	25298
	40	330245	345284	358748	375085

0.95% CNT- 5% CF-RP	2	1.7909	1.8070	1.7872	1.8033
	4	28.691	28.950	28.572	28.830
	10	1115.4	1125.5	1109.8	1119.8
	20	16627	16776	17406	17563
	40	237563	239705	258067	260394
2.85% CNT- 5% CF-RP	2	2.3182	2.3867	2.3135	2.3819
	4	37.139	38.237	36.985	38.079
	10	1443.9	1486.6	1436.6	1479.1
	20	21522	22159	22531	23197
	40	307511	316605	334053	343931
4.75% CNT- 5% CF-RP	2	2.8030	2.9279	2.7973	2.9219
	4	44.906	46.907	44.720	46.713
	10	1745.8	1823.6	1737.0	1814.4
	20	26023	27183	27242	28456
	40	371820	388390	403912	421912
0.9% CNT- 10% CF-RP	2	1.9893	2.0071	1.9852	2.0030
	4	31.870	32.155	31.738	32.022
	10	1239.0	1250.1	1232.8	1243.8
	20	18469	18634	19334	19507
	40	263881	266242	286657	289221
2.7% CNT- 10%CF-RP	2	2.5664	2.6415	2.5611	2.6361
	4	41.115	42.319	40.945	42.144
	10	1598.4	1645.3	1590.4	1636.9
	20	23826	24524	24942	25673
	40	340431	350399	369814	380642
4.5% CNT- 10% CF-RP	2	3.0940	3.2291	3.0877	3.2225
	4	49.568	51.733	49.363	51.519
	10	1927.1	2011.2	1917.3	2001.1
	20	28725	29979	30071	31384
	40	410423	428348	445847	465318

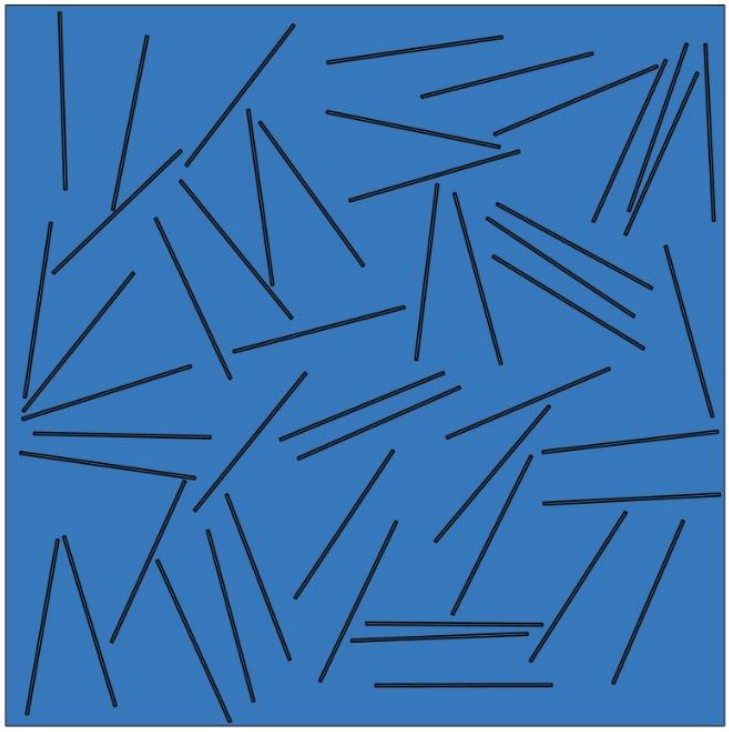

Figure 1: RVE model of composite with random CNT distribution

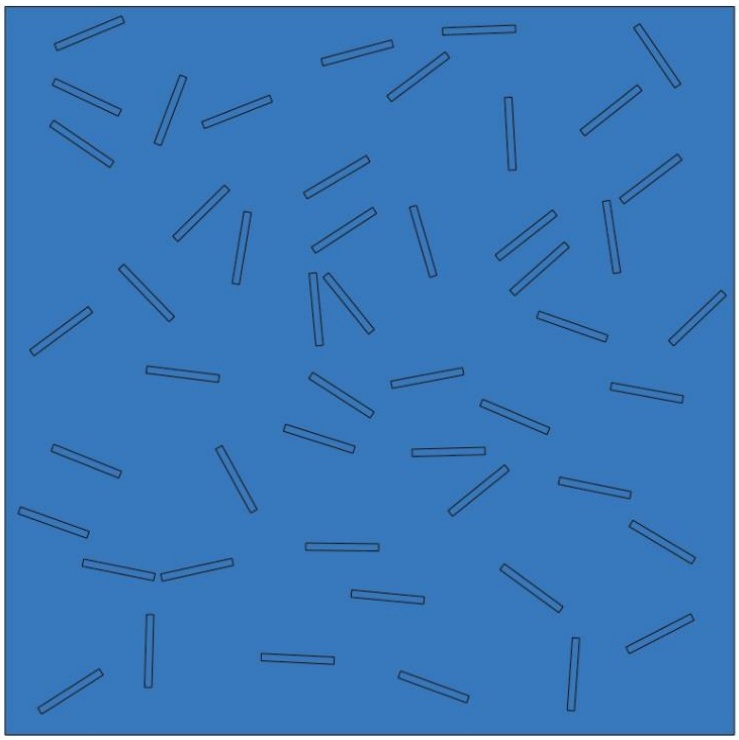

Figure 2: RVE model of composite with random CF distribution

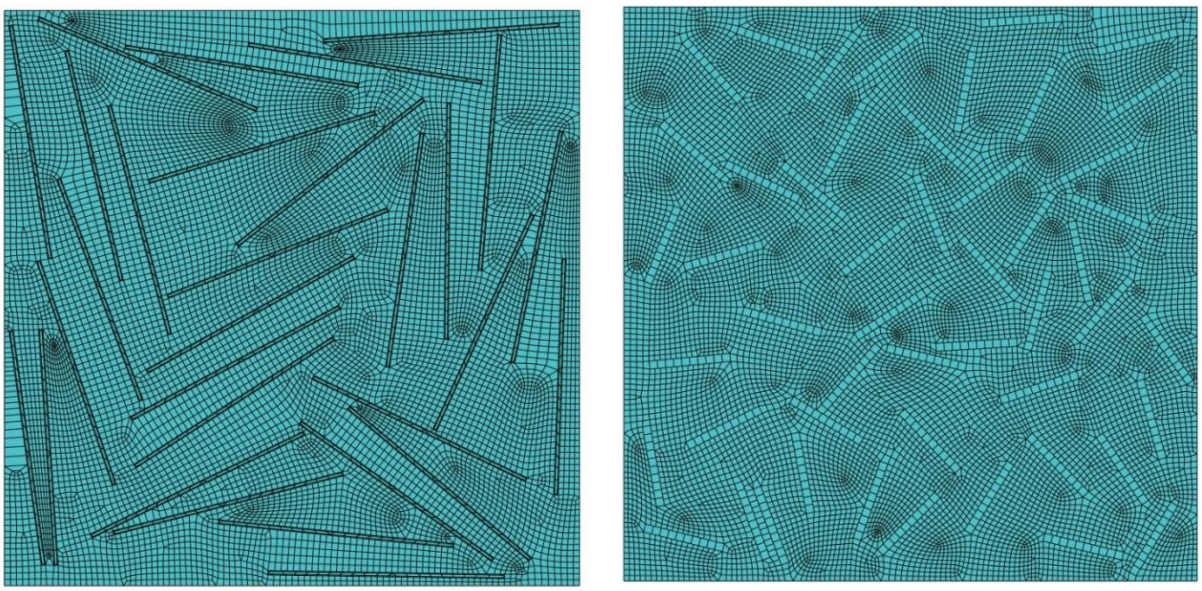

(a) (b)

Figure 3: Examples of meshed RVEs for a) CNT-reinforced polyimide b) CF-reinforced polyimide

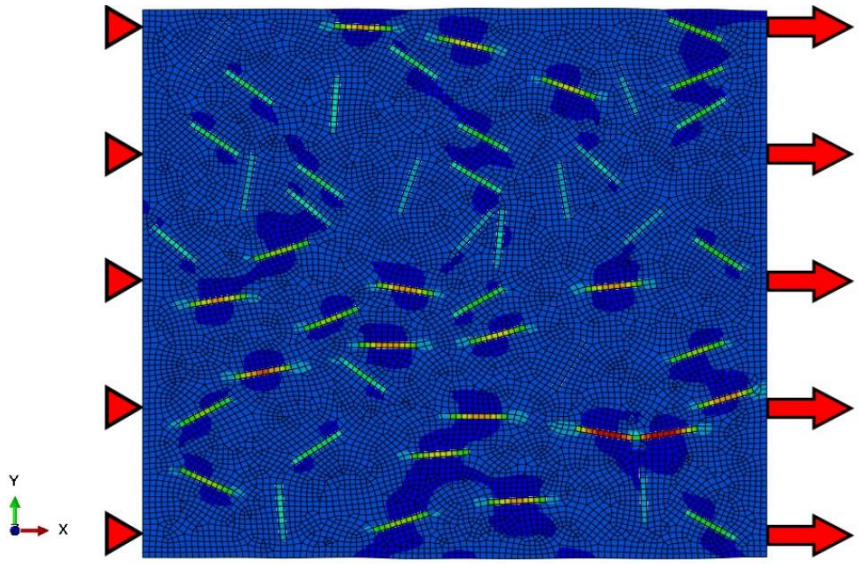

Figure 4: Stress distribution contour (tensile test for obtaining elastic modulus of nanocomposite)

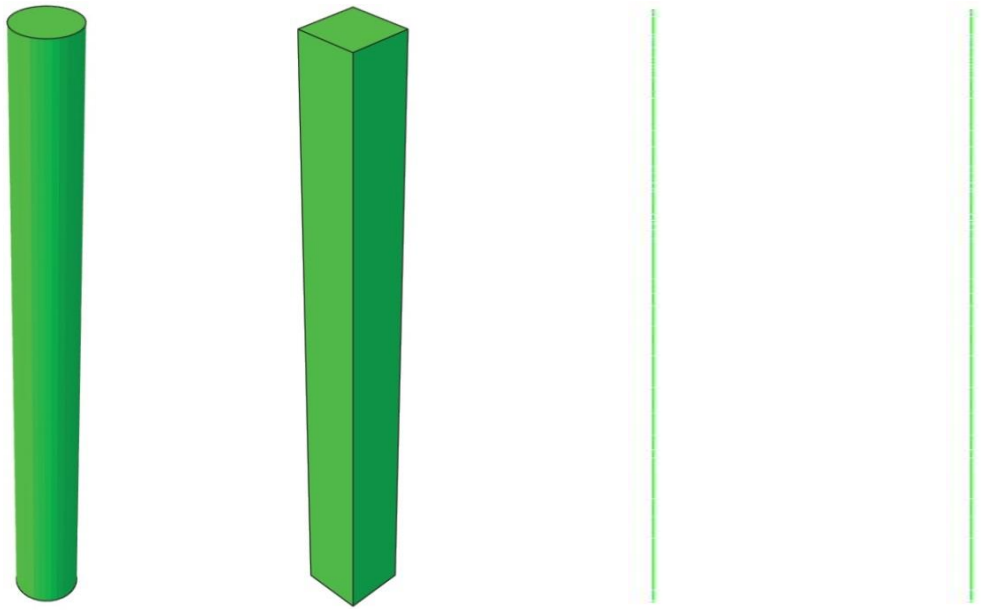

circular cross section Square cross section circular cross section Square cross section

(a) 3D Brick **(b) 2D Beam**

Figure 5: a) 3D brick and b) 2D beam models for the buckling analysis of rods